IOP Publishing Journal of Micromechanics and Microengineering

J. Micromech. Microeng. **17** (2007) 539–550 doi:10.1088/0960-1317/17/3/017

Experimental observations and lattice Boltzmann method study of the electroviscous effect for liquid flow in microchannels

G H Tang, Zhuo Li, Y L He, C Y Zhao and W Q Tao

State Key Laboratory of Multiphase Flow, School of Energy and Power Engineering, Xi'an Jiaotong University, Xi'an, Shaanxi 710049, People's Republic of China

E-mail: ghtang@mail.xjtu.edu.cn

Received 10 October 2006, in final form 14 January 2007
Published 14 February 2007
Online at stacks.iop.org/JMM/17/539

Abstract

The existing experimental data in the literature on hydrodynamics for liquid flow in microchannels are analyzed and the reasons causing the diversities are discussed and summarized. The present experimental data for deionized water flow in glass microtubes with diameters ranging from 50 to 530 μm show that the friction factors and transition Reynolds numbers from laminar to turbulent flow are in good agreement with the conventional theoretical predictions. However, the friction factors in stainless steel microtubes with diameters of 119 and 172 μm are much higher than the conventional theoretical predictions. This discrepancy is attributed to the large surface relative roughness or dense roughness distribution in the stainless steel tubes. Numerical simulations taking into account the electroviscous effect are carried out by using the lattice Boltzmann method. The simulation results show that the electroviscous effect does not play a significant role in the flow characteristics for channel dimensions of the order of microns and hence it can be neglected in engineering applications for moderate electrical conductivity of the liquid and conductivity of the walls. From the literature review and the present test data, it is validated that for liquid flow in smooth microchannels the conventional theoretical prediction for flow characteristics should still be applied.

1. Introduction

In recent years, the application of micro-electro-mechanical-systems has been increasing in many fields due to the rapid development of fabrication technology. Devices with dimensions of the order of microns are being developed for such applications spreading from micro electronic cooling systems to reactors for a range of processes and advanced propulsion systems [1]. A large number of experimental studies have been conducted to investigate the flow and heat transfer characteristics in microchannels, yet differences in the observed friction factor for the liquid flow in microchannels have been reported by many investigators. It is essential to understand the sources of the observed discrepancies in order to avoid them, control them or factor them into the designs. This study makes attempts to tentatively clarify the reasons which can account for such diversities in the measurement of single-phase liquid flow friction characteristics and also examine if conventional theory is still applicable.

In the next part of this section, a comprehensive review on the experimental measurement of liquid hydrodynamics is carried out, and the diversities between different test data are discussed. Based on this review, the reasons that could account for such diversities are summarized.

Lin *et al* [2] studied R12 flow in two copper tubes with diameters of $D = 0.66$ and 1.17 mm and about 20% higher friction factor was obtained than that calculated by using the Blasius equation in Reynolds number range of Re = 4640–

37 600. Urbanek *et al* [3] studied liquid flow (propanol and pentanol) in trapezoidal silicon microchannels with hydraulic diameters of $D_h = 12$ and 25 μm. The experimental results indicated that the friction factor was temperature dependent and increased by 5–30% in the temperature range of 0–85 °C compared to the classical theoretical prediction. Peng *et al* [4] investigated water flow through rectangular stainless steel microchannels with $D_h = 133$–367 μm. Their results indicated that the flow transition from laminar to turbulent occurred at Re = 200–700. The flow friction behaviors of both laminar and turbulent flows were found to deviate from the classical theories. Yang and Webb [5] measured the adiabatic pressure drop of R12 flowing in rectangular multiport aluminum channels of $D_h = 2.64$ mm, and the tested friction factor for the plain channel was approximately 14% higher than that predicted by the Blasius equation.

Papautsky *et al* [6] investigated the deionized water flow in rectangular nickel pipette arrays for Re = 1–20. Each array consisted of five or seven pipettes with widths varying from 150 to 600 μm and heights varying from 22.7 to 26.3 μm and with $\varepsilon/D_h = 0.028\%$. An approximate 20% increase over the classical theory prediction was observed in the friction factor at low aspect ratios. A numerical model of the micropolar fluid theory was presented and the model compared favorably with the experimental data.

Deionized water experiments were conducted by Mala and Li [7] for stainless steel and glass microtubes with $D = 50$–254 μm and relative roughness of $\varepsilon/D = 0.69$–3.5% for Re = 100–2000. On the whole, the experimental results were larger than those predicted by the conventional theory. The deviation increased with the decreasing diameter and the increasing Reynolds number. Qu *et al* [8] investigated the DIUF water flow through trapezoidal silicon microchannels with $D_h = 51.3$–168.9 μm and $\varepsilon/D_h = 1.76$–2.85% for Re < 1500. The friction factor was 8–38% higher than the classical theory prediction. Jiang *et al* [9] tested a micro heat exchanger composed of rectangular copper microchannels with $D_h = 300$ μm and $\varepsilon/D_h = 1.9$–12.1%. The experimental friction factor for water was much higher than the convectional prediction both in laminar and turbulent flow. The transition Reynolds number also occurred much earlier at Re = 600. Celata *et al* [10] studied R114 flow in a stainless steel capillary tube with $D = 130$ μm and $\varepsilon/D = 2.65\%$ for Re = 100–8000. Friction factors were in good agreement with the Hagen–Poiseuille theory for Re < 585. For higher Reynolds numbers, the friction factor deviated from the conventional theory to the higher side.

Pfahler *et al* [11] tested three rectangular silicon microchannels for n-propanol flow. One is 53 μm wide and 135 μm deep and the other two are 100 μm wide and 1.7 and 0.8 μm deep. The friction factor in the 135 μm and 1.7 μm deep channels was found to be in rough agreement with the theoretical prediction. However, for 0.8 μm deep channel it was three times greater than theoretical prediction and decreased with the increase in Reynolds number.

Pfund *et al* [12] conducted experiments for water flow through rectangular microchannels with $D_h = 128$–521 μm for Re = 60–3450. For the channel with $D_h = 521$ μm and $\varepsilon/D_h = 0.57\%$, the friction factor was in rough agreement with the theoretical value and the increase was less than 8%. For three other channels with $\varepsilon/D_h = 1.14$–5.71%, the increase in the friction factor ranged from 10% to 25%. Li *et al* [13] studied the deionized water flow in glass microtubes ($79 < D < 167$ μm and $\varepsilon/D < 0.1\%$), silicon microtubes ($100 < D < 206$ μm and $\varepsilon/D < 0.1\%$) and stainless steel microtubes ($128 < D < 180$ μm and $\varepsilon/D = 3.3$–3.9%) for Re < 4000. For glass and silicon microtubes, friction factors and transition Reynolds numbers were in good agreement with the classical theoretical predictions. For rough stainless steel microtubes, friction factors were 15–37% higher than the theoretical predictions. Phares and Smedley [14] studied water, saline and glycerol/water mixture in four stainless steel tubes with $D = 164$–440 μm and $\varepsilon/D = 2.5$–1.8%, and two polyamide tubes with $D = 119$ and 152 μm and $\varepsilon/D < 1\%$. The measured friction factor in polyamide tubes was in good agreement with the theoretical prediction while the friction factor in stainless steel tubes had 17% deviation to the higher side. Liu and Zhao [15] tested polar fluids (distilled water, ethanol) and non-polar fluid (tetrachloromethane) flowing through stainless steel microtubes with $D = 0.168$, 0.399, 0.799 mm and quartz glass microtubes with $D = 0.242$, 0.315 and 0.52 mm. The experimental results showed that for the tube with $D = 0.168$ mm and $\varepsilon/D = 8$–10%, the value of the friction factor was 10–15% higher than that predicted by the classical theory. The friction factors in other microtubes with relative roughness much less than 3% were in rough agreement with the results by the conventional theory. Kandlikar *et al* [16] studied the microchannel flow of $D_h = 325$–1819 μm at Re = 200–7200 for air and Re = 200–5700 for deionized water. For smooth microchannel with $\varepsilon/D_h = 0.13\%$, the experimental friction factor and transition Reynolds numbers were in good agreement with the conventional theory. For relative roughness of 6–14% based on the constricted flow diameter, the tested friction factors were much higher than the conventional theory.

Reynaud *et al* [17] studied the tap water flow in bronze minichannels. The rectangular channel was very wide and the thickness was 1.12, 0.54 and 0.3 mm with $\varepsilon/D_h = 0.09$, 0.19 and 0.3%, respectively. The friction constant, fRe, was about 96 and in good agreement with the conventional theory for the channels of 1.12 and 0.54 mm thickness, while the tested average value was about 60% higher for the channel of the smallest thickness (0.3 mm). The authors concluded that the experimental results were in good agreement with classical correlations and the observed deviations could be explained either by macroscopic effects (mainly entry and viscous dissipation effects) or by imperfections of the experimental apparatus. The global pressure drop and velocity field were experimentally investigated by Hao *et al* [18] for the water flow in a trapezoidal silicon microchannel with $D_h = 237$ μm and $\varepsilon/D_h = 0.025\%$ for Re = 50–2800. For Re > 700, the relationship of pressure drop and Re deviated from the linear behavior to the higher side and the deviation depended on the Reynolds number. The experimental results of the velocity field showed that the deviation was due to the entrance effect in the microchannel.

Cui *et al* [19] studied the liquid flow in glass microtubes with $D = 3$–10 μm and $\varepsilon/D < 0.7\%$ for Re = 0.1–24. The friction factor for deionized water was in good agreement with the conventional theory while the friction factor for

isopropanol and carbon tetrachloride increased significantly with the increase of the pressure. The authors attributed it to the viscosity increase at high pressure. The authors argued that for most liquids, except for water, the effect of the pressure-dependent viscosity should be considered if the driven pressure was higher than 10 MPa. The revised friction factor taking into account the effect of pressure-dependent viscosity agreed well with the experimental results.

Wilding *et al* [20] analyzed the flow of distilled water and various biological fluids in trapezoidal silicon microchannels varying from 40 to 150 μm in width and from 20 to 40 μm in height. The results suggested that simple liquids behaved both qualitatively and quantitatively according to conventional theories. In contrast to simple fluids, biological fluids exhibited shear-thinning, non-Newtonian behavior. The data indicated an approximately 50% increase in the friction factor from the theoretical values. Mala *et al* [21] investigated the interfacial electrokinetic effects on characteristics of aqueous KC1 solutions and millipore water flow through a microchannel with the height ranging from 10 to 280 μm between two parallel plates with different plate materials, P-type silicon and glass. For the case of small values of zeta potential and high ionic concentrations, the friction constant was approximately 96. But as the zeta potential increased and the ionic concentration decreased, the friction constant also increased. Kulinsky *et al* [22] studied polar and non-polar liquids in trapezoidal silicon channels with $D_h = 3.56$–100 μm. It was found that polar liquids flowed about 6% more slowly than predicted by the classical hydrodynamic theory in the microchannel of $D_h = 90$ μm. For small microchannels with $D_h = 3$–4 μm, the observed retardation was of the order of 70%, while there was no retardation for non-polar octane in the microchannels of $D_h = 90$–100 μm. Collected experimental data had good correspondence with the electrokinetic model presented. Ren *et al* [23,24] and Li [25] studied deionized water, aqueous KCl, $AlCl_3$ and LiCl solutions flow in rectangular silicon microchannels with very large width and heights of 14.1, 28.2 and 40.5 μm and $\varepsilon/D_h =$ 0.07–0.025%. For small ionic concentrations and large values of wall zeta potential, the pressure gradient at the same Reynolds number departed from the conventional predictions to the higher side significantly. The authors attributed it to the electroviscous effect. Brutin and Tadrist [26] studied the distilled and tap water flow in glass microtubes with $D = 50$–530 μm and $\varepsilon/D<0.02\%$. The tested friction factor increased for decreasing microtube diameter and was 27% higher than the conventional theoretical prediction for $D = 50$ μm tube. However, for large tubes and distilled water, the results were close to the conventional theoretical predictions. The authors attributed the friction factor increase to fluid–surface interaction by the fluid ionic coupling with the surface.

Tuckermann and Pease [27] studied the deionized water flow in 287–376 μm deep and 55–60 μm wide rectangular silicon channels. The experimental data lay above and within 5% of conventional theoretical predictions. We classify it as a rough agreement with conventional theory considering the experimental errors. Nakagawa *et al* [28] investigated the deionized water flow in 5 μm deep and 200–800 μm wide rectangular silicon channels. The experimental friction factor agreed within 10% with the conventional theoretical prediction. Bowers and Mudawar [29] tested R113 heated in circular nickel microtubes with $D = 2.54$ and 0.51 mm. The experimental data showed that both single- and two-phase pressure drops in the two tubes could be predicted well by conventional correlations. Horiuchi [30] measured R134a in three plain aluminum tubes with circular multiport channels with $D_h = 0.96$, 1.45 and 2.13 mm. Zhang and Webb [31] also tested R134a flow in rectangular multiport aluminum channels of $D_h = 1.31$ mm. The tested single-phase friction factor was in good agreement with the conventional friction factor correlations. Jiang *et al* [32] presented an experimental investigation of the deionized water flow through silicon microchannels including circular, rectangular and triangular cross-section shapes with $D_h = 8$–24 μm for $Re = 0.1$–2. They found that the friction factor agreed well with the classical theoretical predictions and no geometry influence on flow was observed. Brody *et al* [33] focused on the study of the water flow in a 11 μm deep by 72 μm wide silicon channel. The authors argued that the results obtained demonstrated compliance with the classical hydrodynamic theory. Flockhart and Dhariwal [34] studied distilled water in trapezoidal silicon channels with $D_h = 50$–120 μm for $Re < 600$. The friction results conformed to macro scale laws. Rahman [35] conducted experimental measurements for pressure drop and convective heat transfer in triangle silicon microchannel heat sinks of $D_h = 299$–491 μm with water as a coolant. The measured friction factors were of the same order of magnitude as the conventional predictions for most of the experimental runs. Judy *et al* [36] investigated distilled water, methanol and isopropanol flow in glass and stainless steel microchannels with round and square cross-section shape of $D = 15$–150 μm. Distinguished deviation from classical theory was not observed for $Re = 8$–2300. Yang *et al* [37] provided a systematic test of friction behavior for air, water and R134a in ten tubes with $D = 0.173$–4.01 mm for $Re = 200$–$30\,000$. The friction factors for water and R134a agreed well with the conventional Blasius and Poiseuille equations in turbulent and laminar regimes. Lelea *et al* [38] studied the distilled water behaviors in stainless steel microtubes with $D = 0.1$, 0.3 and 0.5 mm for $Re < 800$. The authors concluded that the classical theories were applicable for the water flow through microchannels of above sizes. Sharp and Adrian [39] performed experiments for deionized water and liquids of different polarities in circular glass microtubes with $D = 50$–247 μm. The measured friction factor and the transition Reynolds number were in agreement with the macroscale predictions for $Re = 50$–3000.

Harms *et al* [40] tested the deionized water flow in a silicon channel of 251 μm wide and 1030 μm deep with $\varepsilon/D_h = 2\%$. The tested friction factors for the laminar and turbulent flows were in rough agreement with the conventional theory. Xu *et al* [41] studied the deionized water flow through rectangular aluminum channels with $46 < D_h < 345$ μm and $\varepsilon/D_h =$ 0.15–1% and silicon channels with $29 < D_h < 79$ μm and $\varepsilon/D_h = 0.025$–0.07% for $20 < Re < 4000$. Rough agreement with conventional theoretical prediction in the friction factor was reported. Gao *et al* [42] studied the demineralized water flow in three rectangular brass microchannels with heights of 0.1–1 mm and the aspect ratio of the channel ranging from

25 to 250 with $\varepsilon/D_h < 0.1\%$ for Re = 20–7400. The friction factor was in good agreement with conventional predictions and the onset to turbulence occurred at a critical Reynolds number in the range of 2500–4000. Li and Cui [43] investigated the non-ion water and organic liquids (CCl_4, $C_6H_5C_2H_5$ and isopropyl alcohol etc) in glass microtubes with $D = 20$ μm and $\varepsilon/D < 0.7\%$. The results showed that the flow rate behaviors for polar or non-polar liquids were in agreement with the conventional theory with the microflow experimental apparatus of pressure range from 0 to 1 MPa. Wu and Cheng [44] measured friction factors of the laminar flow for deionized water in trapezoidal silicon microchannels with $D_h = 25.9$–291 μm and $\varepsilon/D_h < 0.12\%$. The experimental data were found to be in good agreement with the classical predictions. Bucci *et al* [45] studied the water flow in three stainless steel microtubes with $D = 172$, 290 and 520 μm and $\varepsilon/D_h = 0.87\%$, 0.75% and 0.31% for Re = 100–6000. On the whole, the measured friction factor and the transition Reynolds numbers were in rough agreement with the conventional theory. Liu and Garimella [46] investigated the deionized water flow in plexiglass microchannels with $D_h = 244$–974 μm and $\varepsilon/D_h < 3\%$ for Re = 230–6500. Results showed that the conventional theory could be used to successfully predict the flow behavior. Baviere *et al* [47, 48] studied deionized water and a solution of tap water in the deionized water flow in rectangular silicon channels with heights of 21–4.5 μm and $\varepsilon/D_h < 0.5\%$ by using integrated pressure sensors for Re = 0.1–300. The experimental friction factor was in good agreement with the theoretical prediction for conventional channels, regardless of the water electrical conductivity. Kohl *et al* [49] studied compressible flow (air) for $6.8 < \text{Re} < 18\,814$ and incompressible flow (water) for $4.9 < \text{Re} < 2068$ in rectangular silicon channels of $D_h = 25$–100 μm and $\varepsilon/D_h = 0.29$–1.3% with integrated pressure sensors. The experimental results suggested that friction factors for microchannels could be accurately determined from data for standard large channels. Hwang and Kim [50] investigated the pressure drop characteristics of R-134a in stainless steel microtubes with $D = 0.244$, 0.430 and 0.792 mm and $\varepsilon/D = 0.043$–0.16%. Early flow transition from laminar to turbulent was not found and the conventional theory predicted the friction factors for the single-phase flow well within an absolute average deviation of 8.9%.

Pfahler *et al* [51, 52] studied liquid (polar n-propanol and non-polar silicon oil) and gas (nitrogen and helium) flows in ten rectangular and trapezoidal silicon channels with $D_h = 0.96$–39.7 μm and $\varepsilon/D_h < 0.97\%$. Except that the isopropanol flow in the largest channel with $D_h = 39.7$ μm behaved as predicted by the Navier–Stokes equations, the measured friction factor for both liquid and gas was significantly lower than the conventional theoretical values. Hegab *et al* [53] studied refrigerant R134a flow in rectangular aluminum channels with $D_h = 112$–210 μm and $\varepsilon/D_h = 0.16$–0.89% for Re = 1280–13000. For the few data points collected in the laminar regime, the experimental results for the friction factor were very close to predictions using classical laminar flow theory, but in the transition and turbulent regimes, the friction factors were typically 9–23% lower than convectional correlations. Distilled water and nitrogen flows in circular silicon microtubes with $D = 19$, 25 and 102 μm and $\varepsilon/D < 0.03\%$ were reported by Yu *et al* [54]. Water and nitrogen friction factor was about 19% lower than the theoretical value of 64 for $\text{Re} < 2000$. The correlation of fRe = 50.13 was obtained. For turbulent regime of Re = 6000–20 000, the reduction of about 5% in the friction constant was observed.

Guvenc [55] studied the water flow in V-groove silicon capillaries with a width of 50 μm. The measured flow rates were in good agreement with predictions of the conventional theory. In addition, the flow rate increased with the fluid temperature due to the temperature dependence of the viscosity of water. Richter *et al* [56] investigated the water flow in triangle silicon microchannels. The upper width of the channels was varied between 28 and 128 μm, and the depth was determined by the etching angle of 54.7°. The influences of temperature-dependent viscosity were studied for water temperature range of 20–50 °C. At the same pressure drop, the flow rate increased as the temperature increased. The experimental results were in good agreement with the conventional theory if the effect of viscosity dependent on temperature was taken into account. Lim *et al* [57] conducted the deionized water flow in glass microtubes with $D = 49.3$–701.9 μm. For $D < 300$ μm, the friction constant departed from the fully developed fRe of 64 and decreased by 10–25% as the diameter decreased. The authors attributed the decrease in the friction factor to the reduction in the viscosity of water due to viscous dissipation in microtubes. Judy *et al* [58] investigated the effect of the fluid polarity on the frictional characteristics for water, hexane and isopropanol flowing in glass capillaries with $D = 20$–150 μm. The friction factor in the laminar flow was found to be lower than the classical theory for $D < 100$ μm, reaching 30% deviation for the tube of $D = 20$ μm. Qu and Mudawar [59] investigated the deionized water flow in silicon heat sink consisting of an array of 231 μm wide and 713 μm deep rectangular microchannels. A gradual slope change in the pressure drop variation with Reynolds number was attributed to the temperature dependence of water viscosity, and the increasing contraction and expansion pressure losses at the channel inlet and outlet with increasing Reynolds number. For the same Reynolds number, the pressure drop was lower for higher wall heat flux because the higher water temperature under this condition decreased water viscosity. The early transition from laminar to turbulent flow was never observed for Re = 139–1672. The authors argued that the fluid flow and heat transfer within channels with $D_h > 100$ μm and $\text{Re} < 1700$ should follow the conventional theory.

With regard to the thin-film flows, Israelachvili [60] measured the viscosity of tetradecane and NaCl/KCl water solutions in thin films between two flattened molecularly smooth mica surfaces. Gee *et al* [61] measured the viscosity of four hydrocarbon liquids and one silicone liquid similarly. They all found that the film viscosity did not change for thin film flows as long as the film thickness exceeded about 5 nm. Chan and Hon [62] measured the viscosity of three non-polar liquids similarly and they found that the apparent viscosity did not deviate from the fluid viscosity until for films thinner than 50 nm. For thinner film, the apparent viscosity would increase significantly.

We summarized the above-mentioned literature into four categories according to the reported experimental data

compared to conventional theoretical predictions: the one for which the friction factor is larger than the conventional theoretical prediction, the one larger or in rough agreement with the conventional theoretical prediction, the one in rough agreement with the conventional theoretical prediction and the one in rough agreement or lower than the conventional theoretical prediction.

The friction factors were reported to be larger than the conventional theoretical predictions in [2–10]. The measured relative roughness was larger than 1% in [7–10] while no roughness data were reported in [2–5]. Though in [6], the reported relative roughness was much lower than 1%, the authors applied a micropolar theory to explain the larger friction factor.

The friction factors were larger or in rough agreement with the conventional theoretical predictions in [11–26]. The relative roughness was lower than 1% for the channels in rough agreement in [12–19, 23–26]. No roughness data were reported in [11, 20–22]. The relative roughness was larger than 1% for the channels having larger friction factors in [12–16]. Though the roughness was still smaller than 1% in [17–19], the channels having larger friction factors were attributed to the entrance effect in [17, 18] while the larger friction factor in [19] was attributed to the increased water viscosity at a very high pressure of 30 MPa. The larger friction factor in [20–26] was attributed to the electroviscous effect on the polar fluid by the original authors while for non-polar fluid, the friction factor was in good agreement with the conventional theory.

The experimental friction factors were in rough agreement with the conventional theoretical predictions in [27–50]. It can be found that the reported relative roughness was usually less than 1% in [40–50]. The roughness data were not reported in the others.

The experimental friction factors were in rough agreement or smaller than the classical theoretical predictions in [51–59]. It is found that the reported relative roughness was less than 1% in [51–54] while the roughness data were not provided in [55–59]. Due to the liquid viscosity dependent on the temperature, the viscosity decreases as the temperature increases and hence the flow rate increases. The viscous dissipation heating effect will cause the liquid temperature to increase along the streamwise direction, especially for very small size microchannels and high velocity [63]. Hence the lower friction factor could mainly be attributed to the temperature effect on the liquid viscosity. However, it should be noted that the data in [3] are an exception since the reported friction factor increased as the temperature increased.

In summary, we can find that more and more recent results have shown that there are no special microfluidic effects on flow characteristics for single-phase liquid flow in microchannels. Among these results, those of Baviere *et al* [47, 48] and Khol *et al* [49] have to be emphasized. They used integrated pressure sensors and so their results become free from local pressure drops. In addition, we may also tentatively conclude that the higher relative roughness (say, $\varepsilon/D_{\mathrm{h}} > 1\%$) is mainly responsible for the higher friction behaviors for liquid flow in microchannels while the viscous dissipation heating effect or the liquid viscosity dependent on the temperature is mainly responsible for the lower friction behaviors compared to conventional theoretical predictions. Generally speaking, the roughness of metallic microchannels is larger than that of silicon or glass microchannels, and this may account for the fact that the measured friction factor in silicon or glass microchannels is usually smaller than that in metallic microchannels. Apart from the roughness effect to explain the increase in the measured friction factor, the entrance developing effect, inlet and outlet losses, liquid viscosity dependent on high pressure and the electroviscous effect are usually applied to interpret it. It could be easily understood that the entrance developing effect, inlet and outlet losses and liquid viscosity dependent on high pressure would cause the increase in the measured friction factor. However, the electroviscous effect is still disputable. Some researchers did not observe noticeable electroviscous effect regardless of the liquid electrical conductivity. Especially Bavier *et al* [48] pointed out that the actual importance of the electroviscous effect was overestimated for channel size of microns. Regarding the thin-film flows, [60–62] also reported that the film viscosity did not change until below several nanometers.

To further examine the validity of conventional hydrodynamics at microscale, in the following sections, first, experimental investigation was conducted to verify the roughness effect for the DI water flow in smooth and rough microtubes. Second, we applied a lattice Boltzmann method to numerically investigate the electroviscous effect on microflows. Finally, the conclusion is drawn.

2. Experimental study on the roughness effect

2.1. Experimental description

The experimental test system is depicted schematically in figure 1. A high pressure nitrogen gas is connected to the water tank to push the deionized water through the filter, test microtube, flow meter and electronic balance in sequence. A 0.5 μm filter is used to prevent the microtube from possible clotting. The pressure is measured by using pressure transducers with different ranges. The electronic balance is used to measure the flow rate. Also, the volume flow rate is measured by using volume flow meters with different ranges. Two thermocouples at channel inlet and outlet are used to measure the liquid temperature to determine the physical properties. The flow meters, the pressure transducers and the thermocouples are all connected with a computerized data acquisition system.

Four glass circular microtubes and two stainless steel circular microtubes are tested in the experiment. The typical cross-section and longitudinal-section photographs by a scanning electron microscope (SEM) for the test tubes are shown in figure 2. By using light-section microscope, we measured the inner surface relative roughness of the test glass microtubes which is significantly smaller than 1%. And the absolute average surface roughness of the two stainless steel tubes is 7 μm with corresponding relative roughness being 4.1% and 5.9% for the two tubes of $D = 172$ and 119 μm, respectively.

To assess the accuracy of measurement, we performed an uncertainty analysis using the root-sum-square expression

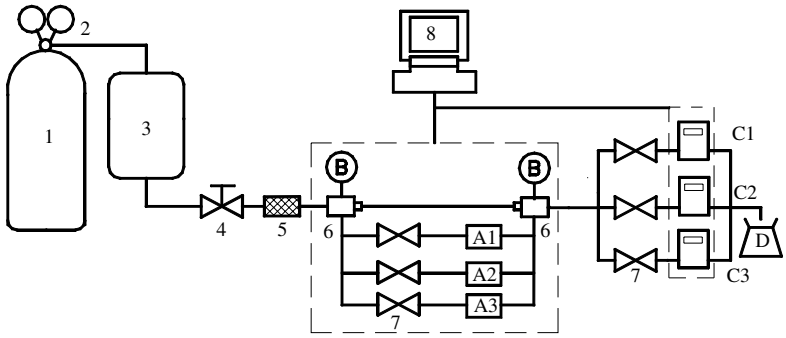

Figure 1. Schematic diagram of the test system for liquid flows. (1) Pressurized tank; (2) regulator; (3) DI water tank; (4) precision regulator; (5) filter; (6) connection adapter for test section; (7) plug valve; (8) data acquisition system; (A1–A3) difference pressure transducers (0–37.4, 0–690, 0–2068 kPa); (B) thermocouples (0–200 °C); (C1–C3) volumetric flow meters (0–1, 0–5, 0–50 ml min^{-1}); (D) electronic balance (0–320 g).

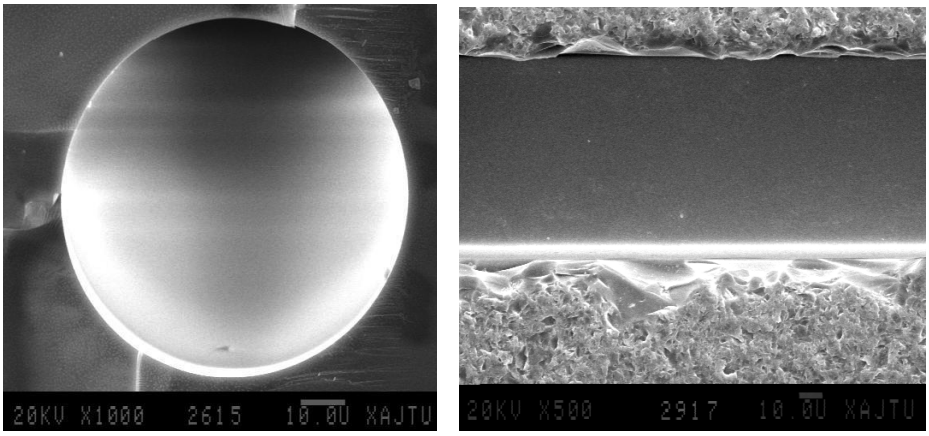

(*a*)

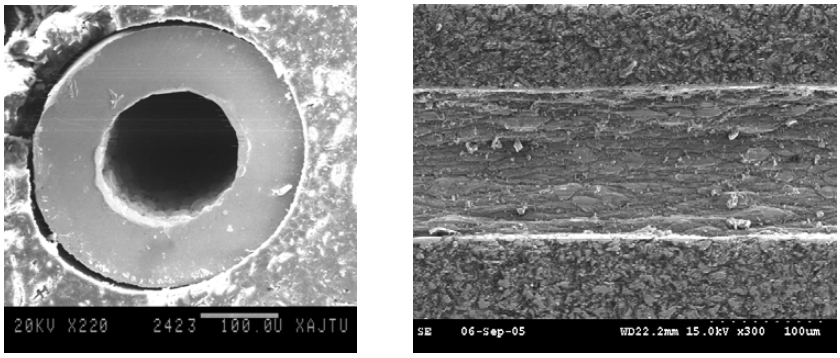

(*b*)

Figure 2. SEM images of three typical tested tubes. (a) A glass microtube with $D = 74$ μm. (b) A stainless steel microtube with $D = 172$ μm.

[64]. The calculated average uncertainty for the Reynolds number and friction factor in the experiments are 4.6% and 6.3%, respectively.

2.2. Experimental results and discussion

In the experiment an isothermal flow is assumed. In fact, due to viscous dissipation effect, a water temperature rise from channel inlet to outlet was observed and the difference increased with fluid velocity, but never exceeded 2 °C in the test. The measured inlet and outlet values were averaged to determine a representative temperature for the fluid.

From the measured mass flow rate, the cross-section average velocity, u_{av}, was determined and the Reynolds number, Re, was calculated as

$$\mathrm{Re} = \frac{\rho u_{\mathrm{av}} D}{\mu}, \tag{1}$$

where ρ is the fluid density and μ is the dynamic viscosity. From the pressure drop across the channel, the Darcy friction factor, f, is calculated by

$$f = \frac{2D\Delta p}{\rho u_{\mathrm{av}}^2 L}, \tag{2}$$

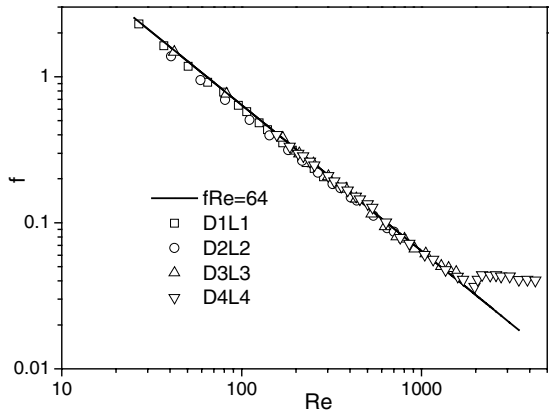

Figure 3. Experimental friction factor for the DI water flow in four glass circular microtubes. D1 = 50.55 μm, L1 = 30.5 mm; D2 = 74.36 μm, L2 = 30.26 mm; D3 = 102.74 μm, L3 = 30.06 mm; D4 = 530.3 μm, L4 = 150.64 mm.

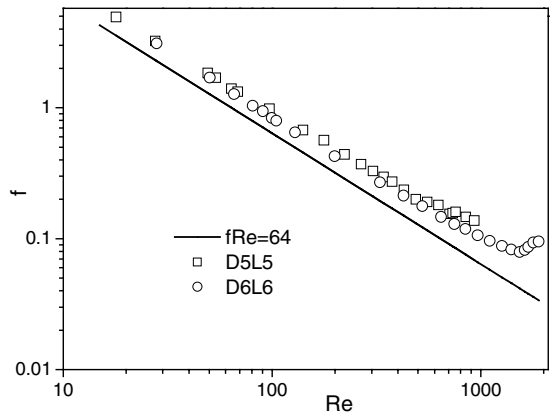

Figure 4. Experimental friction factor for two stainless steel circular microtubes. D5 = 119.09 μm, L5 = 50.40 mm; D6 = 172.0 μm, L6 = 50.54 mm.

where L is the tube length. Note that the measured pressure drop includes the entrance and exit pressure loss. Therefore, the pressure drop in equation (2) should be

$$\Delta p = \Delta p_{\text{measured}} - (k_i - k_o)\,\frac{\rho u_{\text{av}}^2}{2g}, \tag{3}$$

where k_i and k_o are inlet and outlet pressure loss coefficients, respectively, and can be estimated from [65].

The experimental friction factor calculated by equation (2) is plotted against Reynolds number in figures 3 and 4. Figure 3 presents the friction factor for the deionized water flow in glass microtubes with different inner diameters (D) and tube lengths (L). The tested friction factor in microtubes is compared with that from Poiseuille flow prediction for incompressible, laminar flow in a conventional size tube, $f = 64/\text{Re}$. As shown in figure 3, all the experimental results show good agreement with the predictions in the laminar flow regime. The transition Reynolds number from laminar to turbulent flow is about 2000, which is in good agreement with the conventional theory. In figure 4, it is obvious that the friction factors for stainless steel tubes are significantly higher than the conventional theoretical predictions. In addition, the friction factor is larger for the tube of D5 than for the tube of D6. Furthermore, we can also observe that the transition from laminar to turbulent flow occurs earlier about at Re = 1500. We attribute this result to surface roughness effect. Comparing the cross-sections and longitudinal-sections of the SEM photographs for the stainless steel tube with the glass tube shown in figure 2, we find that the inner surface of the stainless steel tubes is quite irregular and many concavo-convex particles are present, while the inner surface of the glass tubes can be regarded as hydraulically smooth. In addition, the measured roughness data also verify this fact. The relative roughness for the stainless steel tube of D5 is larger than for D6 while the relative roughness is very small for all the tested glass microtubes. It should be noted that for nitrogen and helium gaseous flow in glass circular microtubes and square microchannels, the test data were also in good agreement with the conventional theoretical predictions; however, the friction factors for stainless steel microtubes with relative roughness between 2.3% and 5.9% were much higher [66].

3. Lattice Boltzmann method study on the electroviscous effect

It is well known that most solid surfaces carry electrostatic charges, i.e. an electrostatic surface potential. The electrostatic charges on the solid surface will attract the counterions in the liquid when the liquid contains a certain amount of ions. The rearrangement of the charges on the solid surface and the balancing charges in the liquid are called the electrical double layer (EDL) [25, 67]. The EDL is composed of the compact layer strongly attracted to the solid surface and is immobile, normally about 0.5 nm thick, and the diffuse layer, where the ions are less affected by the charged surface and hence are mobile. When liquid flows through a microchannel under a hydrostatic pressure, the nonzero electrical charges in the mobile part of the EDL are carried downstream toward one end, resulting in an electrical current called the streaming current, to flow in the direction of the liquid flow. The accumulation of ions downstream sets up an electrical field with an electrical potential, the streaming potential. This field causes a current, the conductance current, to flow back in the opposite direction until a steady state is reached when the conductance current equals the streaming current. When the ions are moved in the diffuse layer, they pull the liquid along with them in the opposite direction to the pressure-driven flow, leading to a reduced flow rate. For microflows, a phenomenological approach for analyzing the data is to define an apparent viscosity calculated so that if it was used in the conventional Navier–Stokes equations instead of the fluid viscosity. If the reduced flow rate is compared with the prediction from the conventional theory, the effect of the presence of the EDL is similar to that of a liquid having a higher apparent viscosity. Such electrokinetic influence on the flow behavior is referred to as the electroviscous effect [67]. Generally speaking, in the macrochannel flow the electroviscous effect is negligible as the thickness of the EDL is very small compared to the characteristic size of flow channels. However, in the microchannel flow the thickness of the EDL may be comparable to the characteristic size of flow channels. Thus some researchers believe that the electroviscous effect may be significant and should be considered in the study of microchannel flow.

Based on the Debye–Huckel approximation, an exact solution of linear Poisson–Boltzmann equation governing the electrical potential distribution is obtained to describe the electrical double-layer field near the solid/liquid interface. The analytical solution for the modified Navier–Stokes equations was also obtained by using the Green's function formulation by Li and coworkers [21, 25, 68]. Vainshtein and Gutfinger [69] also used a Debye–Huckel linear approximation to consider the EDL effect at the inlet of a parallel channel. The nonlinear Poisson–Boltzmann equation governing the electrical double-layer field was solved numerically with a finite-difference scheme, and modified Navier–Stokes equations were also numerically solved [23, 24, 70] or analytically solved by using the Green's function formulation [71]. Kulinsky *et al* [22] also presented an electrokinetic model for two-dimensional plane channel, and Brutin and Tadrist [72] presented an electrokinetic model for circular tube.

The recent development of the lattice Boltzmann method (LBM) has provided a new simulation tool for computational fluid dynamics [73]. The LBM is different from the conventional numerical methods which solve the usual macroscopic governing equations for the conserved fields. The LBM tries to model the fluid flow by tracking the evolution of the distribution functions of the microscopic fluid particles. That means the LBM provides a method to obtain streaming patterns for complicated systems, which is usually difficult for Navier–Stokes equation-based methods. Li and Kwok [74–77] presented a lattice Boltzmann model in the presence of an externally applied pressure force to describe electrokinetic phenomena using a Poisson–Boltzmann equation.

In the recent work [78, 79], a lattice Boltzmann model for solving both the nonlinear Poisson–Boltzmann equation and the modified Navier–Stokes equation under externally applied electrical fields was proposed. The benefit of this approach is the easiness of programming since the computations of the electric potential fields and the velocity fields are in the same framework of the LBM and have the same structures. Especially this feature could be more useful for a multiprocessor code in parallel computing applications. In this work, based on the LBM model, we investigated the electroviscous effect for liquid flow in microchannels under the externally applied pressure gradient.

3.1. The lattice Boltzmann equation for velocity fields

The discrete lattice Boltzmann equation with the BGK collision approximation including an external force term can be written as [80]

$$f_i(\mathbf{r}+\mathbf{c}_i\delta_t, t+\delta_t) = f_i(\mathbf{r},t) - \frac{1}{\tau_v}\left[f_i(\mathbf{r},t) - f_i^{\mathrm{eq}}(\mathbf{r},t)\right] + \delta_t \frac{\mathbf{F}\cdot(\mathbf{c}_i-\mathbf{u})}{RT} f_i^{\mathrm{eq}}(\mathbf{r},t), \tag{4}$$

where f_i is the single-particle distribution function, τ_v is the non-dimensional relaxation time and $\mathbf{c}_i$ is the particle discrete velocity. For a square lattice D2Q9 model, $\mathbf{c}_0 = 0$ corresponds to the distribution with zero velocity, $\mathbf{c}_i = (\cos[(i-1)\pi/2],\ \sin[(i-1)\pi/2])c$ for $i = 1, 2, 3, 4$, and $\mathbf{c}_i = (\cos[(i-5)\pi/2+\pi/4], \sin[(i-5)\pi/2+\pi/4])c$ for $i = 5, 6, 7, 8$, where $c = \delta_x/\delta_t$ is the particle streaming speed, and δ_x, δ_t are the lattice spacing and step size in time, respectively.

In equation (4) f_i^{eq} $(i = 0, 1, \ldots, 8)$ stands for the equilibrium density distribution function and for the D2Q9 lattice, one obtains the following form [81]:

$$f_i^{eq} = \rho\omega_i\left[1 + \frac{3(\mathbf{c}_i\cdot\mathbf{u})}{c^2} + \frac{9(\mathbf{c}_i\cdot\mathbf{u})^2}{2c^4} - \frac{3(\mathbf{u}\cdot\mathbf{u})}{2c^2}\right], \tag{5}$$

where ω_i is weighting coefficient, having $\omega_0 = 4/9$, $\omega_i = 1/9$ for $i = 1, 2, 3, 4$, and $\omega_i = 1/36$ for $i = 5, 6, 7, 8$. The macroscopic variables such as mass density and the momentum density are defined by sums over the distribution functions $f_i(\mathbf{r}, t)$,

$$\rho = \sum_i f_i, \quad \rho\mathbf{u} = \sum_i f_i\mathbf{c}_i. \tag{6}$$

The kinetic viscosity is

$$\nu = \frac{(2\tau_v - 1)}{6}\frac{\delta_x^2}{\delta_t}. \tag{7}$$

For electroviscous flow only under an externally applied pressure gradient in dilute electrolyte solutions, the external force term can be simplified to

$$\rho\mathbf{F} = -\nabla p - \rho_e\nabla\Phi, \tag{8}$$

where p represents the externally applied pressure, ρ_e represents the net charge density per unit volume at any point in the liquid and Φ is the stream electric potential caused by the ion movements in the solution based on the Nernst–Planck equation. Thus, if the second term on the right-hand side of the above equation is comparable to the applied pressure gradient, we say that the electroviscous effect has a significant effect on the liquid flow in microchannels.

3.2. The lattice Boltzmann equation for electric potential

According to the theory of electrostatics, the relationship between the electric potential in the liquid, ψ, and the net charge density per unit volume, ρ_e, at any point in the liquid is described by the following Poisson equation:

$$\nabla^2\psi = -\frac{\rho_e}{\varepsilon\varepsilon_0}, \tag{9}$$

where ε is the relative dielectric constant of the solution and ε_0 is the permittivity of a vacuum. Assuming that the equilibrium Boltzmann distribution is applicable, the net charge density distribution can be expressed as the sum of all the ions in the solution,

$$\rho_e = \sum_i z_i e n_{i,\infty}\exp\left(-\frac{z_i e\psi}{k_{\mathrm{B}}T}\right), \tag{10}$$

where $n_{i,\infty}$ and z_i are the bulk ionic concentration and the valence of type i ion, respectively. The bulk ionic concentration n_∞ can be expressed as the product of the ionic molar concentration of c_∞ with the Avogadro's number of N_0. Constant e is the charge of a proton, k_{B} is the Boltzmann constant and T is the absolute temperature. Substituting equation (10) into equation (9) yields the nonlinear Poisson–Boltzmann equation,

$$\nabla^2\psi + \frac{1}{\varepsilon\varepsilon_0}\sum_i z_i e n_{i,\infty}\exp\left(-\frac{z_i e\psi}{k_{\mathrm{B}}T}\right) = 0. \tag{11}$$

We can obtain the following discrete lattice Boltzmann evolution equation for the electric potential [79]:

$$g_i(\mathbf{r}+\mathbf{c}_i\delta_{t,g}, t+\delta_{t,g}) = g_i(\mathbf{r},t) - \frac{\delta_{t,g}}{\tau_g+0.5\delta_{t,g}}\left[g_i(\mathbf{r},t)-g_i^{\mathrm{eq}}(\mathbf{r},t)\right] + \left(\frac{\tau_g}{\tau_g+0.5\delta_{t,g}}\right) \times \left(\frac{1}{\varepsilon\varepsilon_0}\sum_i z_i e n_{i,\infty}\exp\left(-\frac{z_i e\psi}{k_B T}\right)\right)\delta_{t,g}\omega_i. \quad (12)$$

The corresponding equilibrium distribution of g^{eq} on the D2Q9 discrete lattice takes the form $g_0^{\mathrm{eq}} = 0$, $g_{1,2,3,4}^{\mathrm{eq}} = \psi/6$ and $g_{5,6,7,8}^{\mathrm{eq}} = \psi/12$.

The potential diffusivity χ, which is equal to unity in the simulations, is defined as

$$\chi = \frac{2\tau_g}{3}\frac{\delta_x^2}{\delta_{t,g}}. \quad (13)$$

The macroscopic electric potential in the liquid is calculated as

$$\psi = \sum_i g_i + \frac{\delta_{t,g}}{2}\sum_i\left(\frac{1}{\varepsilon\varepsilon_0}\sum_i z_i e n_{i,\infty}\exp\left(-\frac{z_i e\psi}{k_B T}\right)\right)\omega_i. \quad (14)$$

The present LBM method is relatively simple and can be straight extended to three-dimensional problems by using D3Q15 or D3Q19 lattice models, and, in particular, it is of good numerical stability and flexibility to deal with complex geometries, since general boundary conditions are easily implemented without special attention.

If assuming uniform dielectric constant and neglecting the fluctuation of the dielectric constant, in other words, the ion-convection effects will be relatively smaller than the ion diffusion effects, and can be neglected when the Peclet number is smaller than 100 [82], the net charge density distribution is proportional to the concentration difference between the cations and anions,

$$n_{\pm} = n_\infty \exp\left(\mp\frac{ze\psi}{k_{\mathrm{B}}T}\right), \quad (15)$$

$$\rho_e = ze\,(n_+ - n_-) = -2zen_\infty \sinh\left(\frac{ze\psi}{k_{\mathrm{B}}T}\right), \quad (16)$$

and thus it yields the following nonlinear Poisson–Boltzmann equation for the electrical potential in the dilute electrolyte solution,

$$\nabla^2\psi = \frac{2zen_\infty \sinh\left(\frac{ze\psi}{k_{\mathrm{B}}T}\right)}{\varepsilon\varepsilon_0}. \quad (17)$$

If $ze\psi/k_{\mathrm{B}}T$ is small, we have $\sinh(ze\psi/k_{\mathrm{B}}T)\approx ze\psi/k_{\mathrm{B}}T$ based on the Debye–Huckel approximation. Equation (17) recovers the so-called linearized Poisson–Boltzmann equation. However, in the present study, we still solve the nonlinear Poisson–Boltzmann equation.

The stream electric potential can be obtained through a balance between streaming current and electrical conductance current at steady state

$$\Phi = -\frac{\rho_e u}{\lambda_0 + \lambda_s/(A_c/P)}, \quad (18)$$

where P and A_c are the wetting perimeter and the cross section area of the channel, respectively. For a two-dimensional parallel channel, we have $A_c/P = H/2$, and H is the channel height. Here λ_0 is the electrical conductivity of the bulk liquid and λ_s is the surface conductance of the wall. The electrostatic surface potential at the walls ψ_s, λ_0 and λ_s can be determined by experiments. ψ_s and λ_s are found to vary for different surface materials and electrolyte solutions [21].

With regard to the boundary condition, we adopted the non-slip boundary conditions by Zou and He [83] on the upper and bottom walls to solve the density distribution function for velocity fields. For the lattice Boltzmann equation for the electric potential, the zeta potentials on the upper and bottom walls are known in the simulation and we employed the Dirichlet boundary condition in our previous work [84]. For the channel inlet and the outlet, we employed periodic boundary conditions by assuming a fully developed flow. This LBM model for nonlinear Poisson–Boltzmann equation has been well validated by comparing the LBM results with analytical solutions when the zeta potential is small based on the Debye–Huckel approximation, and with the numerical results of the finite volume method for relatively large zeta potentials [79]. In addition, the LBM model for velocity fields has also been well validated by comparing the LBM results with analytical solutions of Womersley flow.

3.3. The LBM simulation results and discussion

In this paper, the simulated prototypes are copied from the experimental works by Ren *et al* [24] and Baviere *et al* [48]. Note that the rectangular channels in [24, 48] have very large ratios of width to height; the channel heights (H) for the two-dimensional parallel channels presented here are slightly adjusted by calculating the corresponding hydraulic diameters.

In the simulation, the flow is assumed to be laminar fully developed, and in steady state. The fluid density and dynamic viscosity are considered to be constant at 21 °C, $\rho =$ 997.94 kg m^{-3}, and $\mu = 983.75 \times 10^{-6}$ kg m^{-1} s^{-1}. The simulated microchannels are made of silicon, and the relative roughness of channels is much less than 1%. The very low relative roughness of these channels implies that the roughness effect can be ignored in the simulation model.

Since the experimental data were not tabulated, Li and Kwok [74] digitized the experimental results from the figures in [24]. Now we use their digitized data for comparison. The model predictions together with the experimental data are shown in tables 1 and 2 for $H = 14.06$ and 28.04 μm, respectively. The test liquids are DIUF water and KCl solution. We can see that compared to the analytical solutions for a fully developed pure pressure-driven laminar flow at the same pressure gradient, the Reynolds number and the friction constant calculated by the LBM have a quite small deviation less than 2%. The deviation is lower for the large channel than for the small channel, and lower for that with high ionic concentration and low zeta potential than for that with small ionic concentration and large zeta potential. However, the largest decrease in Reynolds number of about 20% was observed in the experiment [24]. The present LBM simulation results cannot reproduce the experimental results. In table 1, we also calculated the Reynolds number and the friction constant without considering electroviscous effect using the LBM; we can see that both

Table 1. Comparison of the experimental data for dp/dx versus Re in [24] with the LBM results for channel height $H = 14.06$ μm.

dp/dx (10^6 Pa m^{-1}) (Exp [24])	Re (Exp [24])	Re/fRe (LBM)	Re/fRe (pure pressure driven, analytical)	Re/fRe (pure pressure driven, LBM)
DIUF water, $n_\infty = 10^{-6}$ M, $\zeta = 245$ mV, $\lambda_s = 2.43 \times 10^{-8}$ S, $\lambda_0 = 1.053 \times 10^{-4}$ S m^{-1}				
2.35	0.98	1.1/97.98	1.122/96	1.121/96.02
3.08	1.28	1.442/97.98	1.471/96	1.47/96.02
3.71	1.52	1.738/97.98	1.772/96	1.769/96.02
4.43	1.79	2.073/97.98	2.116/96	2.113/96.02
KCl solution, $n_\infty = 10^{-4}$ M, $\zeta = 107$ mV, $\lambda_s = 1.76 \times 10^{-7}$ S, $\lambda_0 = 1.5025 \times 10^{-3}$ S m^{-1}				
2.28	1.04	1.07/97.64	1.089/96	
3.04	1.29	1.428/97.64	1.452/96	
3.60	1.54	1.688/97.64	1.719/96	
4.29	1.85	2.011/97.64	2.049/96	

Table 2. Comparison of the experimental data for dp/dx versus Re in [24] with the LBM results for channel height $H = 28.04$ μm.

dp/dx (10^6 Pa m^{-1})	Re (Exp [24])	Re/fRe (LBM)	Re/fRe (pure pressure driven, analytical)
DIUF water, $n_\infty = 10^{-6}$ M, H = 28.04 μm, $\zeta = 245$ mV, $\lambda_s = 7.48 \times 10^{-8}$ S, $\lambda_0 = 1.053 \times 10^{-4}$ S m^{-1}			
2.68	8.62	10.097/96.54	10.154/96
3.16	10.77	11.906/96.54	11.973/96
3.69	12.92	13.903/96.54	13.981/96
4.18	15.15	15.749/96.54	15.838/96
4.71	17.38	17.746/96.54	17.846/96
KCl solution, $n_\infty = 10^{-4}$ M, 28.04 μm, $\zeta = 107$ mV, $\lambda_s = 4.15 \times 10^{-7}$ S, $\lambda_0 = 1.5025 \times 10^{-3}$ S m^{-1}			
2.58	8.62	9.725/96.50	9.775/96
3.08	10.77	11.609/96.50	11.67/96
3.58	12.92	13.494/96.50	13.564/96
4.08	15.15	15.379/96.50	15.459/96
4.58	17.38	17.263/96.50	17.353/96

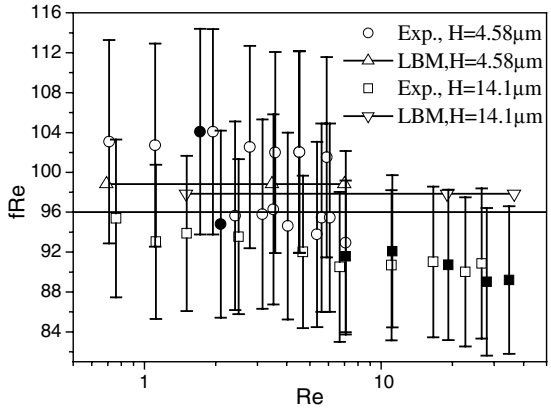

Figure 5. The LBM simulation results compared with experimental data [48]. Open symbols: DI water. Solid symbols: tap water.

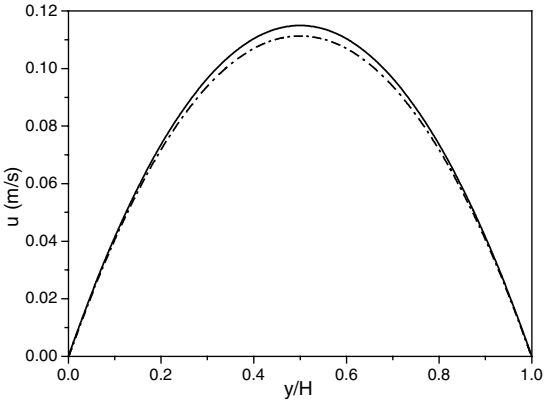

Figure 6. Velocity profile of pressure-driven flow with the electroviscous effect compared to analytical solution without the electroviscous effect (dp/dx = 45 MPa).

the Reynolds number and the friction constant are in good agreement with the analytical solutions for a pure pressure-driven laminar flow in the fully developed region. This agreement also validates the present LBM code.

Second, we compared the DIUF water flow in two channels presented by Baviere *et al* [48], $H = 4.484$ μm and $H = 14.1$ μm. Because the zeta potential and the properties of the bulk liquid were not measured in [48], we adopted the properties of the DIUF water which may cause the largest electroviscous effect presented by Ren *et al* [24] for an approximation comparison, $n_\infty = 10^{-6}$ M, $\zeta = 245$ mV, $\lambda_s = 2.43 \times 10^{-8}$ S, $\lambda_0 = 1.053 \times 10^{-4}$ S m^{-1}. The friction factors of the experimental data and the computed LBM results are shown in figure 5. We can see that the experimental data and the present LBM results are in good agreement with the analytical solutions for a pure pressure-driven flow (fRe = 96), the largest deviation for the LBM results from the value of fRe = 96 is less than 3% for the channel with $H = 4.484$ μm, and less than 2% for the channel with $H = 14.1$ μm.

Figure 6 shows the velocity profile from the LBM simulation for the DIUF water flow in the channel with $H = 4.484$ μm. The dash dot represents the LBM results for the pressure-driven flow with electroviscous effect, and the solid line represents the analytical solution for a pure pressure-driven flow without electroviscous effect. As we can see, the velocity with electroviscous effect is slightly smaller than that without electroviscous effect. The velocity result

is consistent with the calculated friction constant, which is 98.83 for the channel with $H = 4.484$ μm. On the whole, the present numerical study shows that the increase in the friction factor or the decrease in Reynolds number resulting from the electroviscous effect is usually within the range of experimental uncertainties and can be neglected in engineering applications.

4. Conclusions

We summarized the reasons causing the differences of hydrodynamic characteristics for liquid flow in microchannels through a large number of experimental observations. These differences may be due to imperfections in the flow system of the experiment, including the measurement of the inner size of the microchannel, developing entrance effect, the inlet and exit minor losses due to the measured whole pressure drop in most experiments, non-uniform flow rate distribution in the test for multiport microchannels and the possible dissolved gas in the liquid since most investigators applied a high gas pressure to push the liquid flowing through the microchannels. Apart from these imperfections, the higher surface relative roughness and the liquid viscosity dependent on high pressure are usually responsible for the deviation to the higher side, while viscous dissipation heating effect or the liquid viscosity dependent on temperature are usually responsible for the deviation to the lower side.

In addition, the present experimental data for the deionized water flow in circular microtubes with $50 < D < 530$ μm have verified that the roughness is mainly responsible for the higher friction factors. The friction factors and the transition Reynolds number from laminar to turbulent flow for smooth channels are in good agreement with the conventional theoretical predictions while significant deviations to the higher side are observed for the rough channels. The present simulation results by using the lattice Boltzmann method have shown that the electroviscous effect does not play a significant role in the flow characteristics for channel dimensions of the order of microns and hence it can be ignored in engineering applications for moderate electrical conductivity of the liquid and conductivity of the walls. From the literature review and the present test data, it is validated that for liquid flow in smooth microchannels the conventional theoretical prediction for flow characters should still be applied. It should be noted that our study is limited to the channel size of microns. For nanometer dimensions, the surface tension, van der Waals forces, contact angle between the liquid and solid surface and other capillary wall–fluid interactions may dominate the flow and should be taken into account.

Acknowledgments

This work was supported by the National Natural Science Foundation of China (grant nos. 50406020, 50425620, 50576069) and the National Fundamental Research Program of China (grant no. 2006CB601203).

References

[1] Gad-el-Hak M 1999 *J. Fluids Eng.* **121** 5–33
[2] Lin S, Kwok C C K, Li R Y, Chen Z H and Chen Z Y 1991 *Int. J. Multiph. Flow* **17** 95–102
[3] Urbanekt W, Zemel J N and Bau H 1993 *J. Micromech. Microeng.* **3** 206–8
[4] Peng X F, Peterson G P and Wang B X 1994 *Exp. Heat Transfer* **7** 249–64
[5] Yang C Y and Webb R L 1996 *Int. J. Heat Mass Transfer* **39** 801–9
[6] Papautsky I, Brazzle J, Ameel T and Frazier A B 1999 *Sensors Actuators* **73** 101–8
[7] Mala G M and Li D Q 1999 *Int. J. Heat Fluid Flow* **20** 142–8
[8] Qu W L, Mala G M and Li D Q 2000 *Int. J. Heat Mass Transfer* **43** 353–64
[9] Jiang P X, Fan M H, Si G S and Ren Z P 2001 *Int. J. Heat Mass Transfer* **44** 1039–51
[10] Celata G P, Cumo M, Guglielmi M and Zummo G 2002 *Microscale Thermophys. Eng.* **6** 85–97
[11] Pfahler J, Harley J and Bau H 1990 *Sensors Actuators* **A21–A23** 431–4
[12] Pfund D, Rector D, Shekarriz A, Popescu A and Welty J 2000 *AIChE J.* **46** 1496–07
[13] Li Z X, Du D X and Guo Z Y 2003 *Microscale Thermophys. Eng.* **7** 253–65
[14] Phares D J and Smedley G T 2004 *Phys. Fluids* **16** 1267–72
[15] Liu Z G and Zhao Y H 2005 *J. Univ. Shanghai Sci. Technol.* **27** 123–6 (in Chinese)
[16] Kandlikar S G, Schmitt D, Carrano A L and Taylor J B 2005 *Phys. Fluids* **17** 100606–11
[17] Reynaud S, Debray F, Franc J P and Maitre T 2005 *Int. J. Heat Mass Transfer* **48** 3197–211
[18] Hao P F, He F and Zhu K Q 2005 *J. Micromech. Microeng.* **15** 1362–8
[19] Cui H H, Silber-Li Z H and Zhu S N 2004 *Phys. Fluids* **16** 1803–10
[20] Wilding P, Shoffner M A and Kircka L J 1994 *Clin. Chem.* **40** 43–7
[21] Mala G M, Li D Q, Werner C, Jacobasch H J and Ning Y B 1997 *Int. J. Heat Fluid Flow* **18** 489–96
[22] Kulinsky L, Wang Y and Ferrari M 1999 Electroviscous effects in microchannels *SPIE Conf. on Micro- and Nanofabricated Structures and Devices for Biomedical Environmental Applications II (San Jose, CA)* vol 3606 pp 158–68
[23] Ren L Q, Li D Q and Qu W L 2001 *J. Colloid Interface Sci.* **233** 12–22
[24] Ren L Q, Qu W L and Li D Q 2001 *Int. J. Heat Mass Transfer* **44** 3125–34
[25] Li D Q 2001 *Colloids Surf.* A **195** 35–57
[26] Brutin D and Tadrist L 2003 *Phys. Fluids* **15** 653–61
[27] Tuckermann D B and Pease R F W 1982 *J. Electrochem. Soc.* **129** C98
[28] Nakagawa S, Shoji S and Esashi M 1990 A micro chemical analyzing system integrated on silicon chip *Proc. IEEE: Micro Electro Mechanical Systems (Napa Valley CA)* pp 89–94
[29] Bowers M B and Mudawar I 1994 *Int. J. Heat Mass Transfer* **37** 321–32
[30] Horiuchi H 1995 Test report on extruded aluminum tubes *Penn. State University Report to Showa Aluminum Co.*
[31] Zhang M and Webb R L 1997 Effect of oil on R-134a condensation in parallel flow condensers *SAE 1997 Vehicle Thermal Management Systems Conf.* pp 369–76
[32] Jiang X N, Zhou Z Y, Yao J, Li Y and Ye X Y 1995 Micro-fluid flow in microchannels *The 8th Int. Conf. on Solid-State Sensors and Actuators and Erosensors* vol IX pp 317–20
[33] Brody J P, Yager P, Goldstein R and Austin R H 1996 *Biophys. J.* **71** 3430–41
[34] Flockhart S M and Dhariwal R S 1998 *ASME J. Fluids Eng.* **120** 291–5
[35] Rahman M M 2000 *Int. Commun. Heat Mass Transfer* **27** 495–506

[36] Judy J, Maynes D and Webb B W 2005 *Int. J. Heat Mass Transfer* **45** 3477–89
[37] Yang C Y, Wu J C, Chien H T and Lu S R 2003 *Microscale Thermophys. Eng.* **7** 335–48
[38] Lelea D, Nishio S and Takano K 2004 *Int. J. Heat Mass Transfer* **47** 2817–30
[39] Sharp K V and Adrian R J 2004 *Exp. Fluids* **36** 741–7
[40] Harms T M, Kazmierczak M, Gerner F M, Holke A, Henderson H T, Pilchowski J and Baker K 1997 Experimental investigation of heat transfer and pressure drop through deep microchannels in a (110) silicon substrate *Proc. ASME Heat Transfer Division* vol 351–1 pp 347–57
[41] Xu B, Ooi K T, Wong N T and Choi W K 2000 *Int. Commun. Heat Mass Transfer* **27** 1165–76
[42] Gao P, Person S L and Favre-Marinet M 2002 *Int. J. Therm. Sci.* **41** 1017–27
[43] Li Z H and Cui H H 2002 *Int. J. Nonlinear Sci. Numer. Simul.* **3** 577–80
[44] Wu H Y and Cheng P 2003 *Int. J. Heat Mass Transfer* **46** 2519–25
[45] Bucci A, Celata G P, Cumo M, Serra E and Zummo G 2003 Fluid flow and single-phase flow heat transfer of water in capillary tubes *Proc. 1st Int. Conf. Minichannels and Microchannels (Rochester, USA)* Paper ICMM-1037
[46] Liu D and Garimella S V 2004 *AIAA J. Thermophys. Heat Transfer* **18** 65–72
[47] Baviere R and Ayela F 2004 *Meas. Sci. Technol.* **15** 377–83
[48] Baviere R, Ayela F, Le Person S and Favre-Marinet M 2005 *Phys. Fluids* **17** 098105–4
[49] Kohl M J, Abdel-Khalik S I, Jeter S M and Sadowski D L 2005 *Int. J. Heat Mass Transfer* **48** 1518–33
[50] Hwang Y W and Kim M S 2006 *Int. J. Heat Mass Transfer* **49** 1804–12
[51] Pfahler J, Harley J, Bau H H and Zemel J N 1990 Liquid and gas transport in small channel *Micro Structures, Sensors, and Actuators ASME DSC* vol 19 pp 149–57
[52] Pfahler J, Harley J, Bau H H and Zemel J N 1991 Gas and Liquid flow in small channel *Micromechanical Sensors, Actuators, and Systems ASME DSC* vol 32 pp 49–60
[53] Hegab H, Bari A and Ameel T 2002 *Exp. Heat Transfer* **15** 245–59
[54] Yu D, Warrington R, Barron R and Ameel T 1995 An experimental and theoretical investigation of fluid and heat transfer in microtubes *Proc. 4th ASME/JSME Thermal Engineering Joint Conf.* vol 1 pp 523–30
[55] Guvenc M G 1985 V-groove capillary for low flow control and measurement *Micromachining and Micropackaging of Transducers* ed C D Fung, P W Cheung, W H Ko and D G Fleming (Amsterdam: Elsevier) pp 215–23
[56] Richter M, Woias P and Weib D 1997 *Sensors Actuators* A **62** 480–3
[57] Lim S K, Ooi K T, Wong T N, Toh K C and Suzuki K 2000 Experimental investigation of liquid flow in a micro-tube *Engineering Advances at the Dawn of the 21st Century: Proc. Seminar on Integrated Engineering* pp 487–93
[58] Judy J, Maynes D and Webb B W 2000 Liquid flow pressure drop in microtubes *Proc. Int. Conf. Heat Transfer and Transport Phenomena in Microscale (Banff, Canada, 15–20 Oct.)* pp 149–54
[59] Qu W and Mudawar I 2002 *Int. J. Heat Mass Transfer* **45** 2549–65
[60] Israelachvili J N 1986 *J. Colloid Interface Sci.* **110** 263–71
[61] Gee M L, McGuiggan P M, Israelachvili J N and Homola A M 1990 *J. Chem. Phys.* **93** 1895–906
[62] Chan D Y C and Horn R G 1985 *J. Chem. Phys.* **83** 5311–24
[63] Koo J and Kleinstreuer C 2003 *J. Micromech. Microeng.* **13** 568–79
[64] Abernethy R B, Benedict R P and Dowdell R B 1985 *ASME J. Fluids Eng.* **107** 161–4
[65] Streeter V L and Wylie E B 1985 *Fluid Mechanics* 8th edn (New York: McGraw-Hill)
[66] Tang G H, Li Z, He Y L and Tao W Q 2007 *Int. J. Heat Mass Transfer* at press (doi:10.1016/j.ijheatmasstransfer.2006.10.034)
[67] Hunter R J 1981 *Zeta Potential in Colloid Science: Principles and Applications* (New York: Academic)
[68] Yang C and Li D Q 1998 *Colloids Surf.* A **143** 339–53
[69] Vainshtein P and Gutfinger C 2002 *J. Micromech. Microeng.* **12** 252–6
[70] Chen X Y, Toh K C, Chai J C and Yang C 2004 *Int. J. Eng. Sci.* **42** 609–22
[71] Yang C and Li D Q 1997 *J. Colloid Interface Sci.* **194** 95–107
[72] Brutin D and Tadrist L 2005 *Microscale Thermophys. Eng.* **9** 33–48
[73] Chen S and Doolen G D 1998 *Annu. Rev. Fluid. Mech.* **30** 329–64
[74] Li B M and Kwok D Y 2003 *Int. J. Heat Mass Transfer* **46** 4235–44
[75] Li B M and Kwok D Y 2003 *J. Colloid Interface Sci.* **263** 144–51
[76] Li B M and Kwok D Y 2003 *Langmuir* **19** 3041–8
[77] Li B M and Kwok D Y 2004 *J. Chem. Phys.* **120** 947–53
[78] Wang J K, Wang M and Li Z X 2006 *J. Colloid Interface Sci.* **296** 729–36
[79] Tang G H, Li Z, Wang J K, He Y L and Tao W Q 2006 *J. Appl. Phys.* **100** 094908-10
[80] He X Y and Luo L S 1997 *Phys. Rev.* E **56** 6811–7
[81] Qian Y H, d'Humieres D and Lallemand P 1992 *Europhys. Lett.* **17** 479–84
[82] Rice C L and Whitehead R 1965 *J. Phys. Chem.* **69** 4017–24
[83] Zou Q and He X Y 1997 *Phys. Fluids* **9** 1591–8
[84] Tang G H, Tao W Q and He Y L 2005 *Phys. Rev.* E **72** 016703-6